Mechanical Design Process for the Zippy Wrist

BSME, Navid Mahpeykar, Ferdowsi University of Mashhad, M.E Department, Iran
PhD, Javad Enferadi, Ferdowsi University of Mashhad, M.E Department, Iran
PhD, Alireza Akbarzadeh, Ferdowsi University of Mashhad, M.E Department, Iran

Abstract

In this paper, the mechanical design process of a star spherical parallel robot that we call Zippy Wrist is illustrated. The Zippy Wrist is a 3-RRP spherical parallel manipulator and can perform many industrial applications such as; orienting a tool or a workpiece in machine tools, solar panels, space antennas and telescopic mechanisms, flight simulator mechanism and camera devices. The forward and inverse kinematics problem, isotropy design, singularity analysis, accuracy analysis, stiffness analysis, inverse and direct dynamic analysis of this manipulator have previously been investigated by Enferadi and Akbarzadeh and reported in four journals [1,2,3,4]. Our goal was to build a laboratory version of the Zippy Wrist to test theoretical results and to perform additional dynamical and control testing. The selected mechanical design is based on the isotropic design because it is the superior design. The design results in a relatively large workspace, good accuracy and high stiffness [1]. The mechanical design process consists of joints design, structural analysis of main components, geometry determination of components, material selection and safety issues. The controller allows PID control as well as running the system in torque mode. This allows us to directly input the calculated torque, from robot dynamic equations to motors. Structural analysis is performed by finite element models considering load capacity and other design goals. Dynamic and motion of the robot is simulated using hypothetical trajectories to obtain desired kinematic parameters such as speed and acceleration. The robot is assumed to carry an average load of 1kg, mostly due to carrying measurement tools such as accelerometer, laser tool or camera. All mechanical components are designed using commercial solid modelling software and manufacturing processes are briefly discussed.

1 Introduction

Orientating a rigid body without changing its position is required in many technical applications. A spherical manipulator is one in which the end effector is moved on the surface of a sphere. Therefore, a spherical manipulator can be used as a device to orient the end effector. Spherical manipulators can be either serial [5] or parallel [6,7,8]. Serial manipulators feature an open kinematics chain which ending link is the end-effector. Parallel manipulators consisted of two rigid bodies, one moveable (platform) and the other fixed (base), connected to each other by a number of kinematics chains (legs). The moving platform and the fixed base are respectively the end-effector and the base frame. In each leg, the number of actuated kinematics pairs is less than the total number of kinematics pairs. All legs contribute in carrying the external loads applied to the moving platform. These attributes lead to high stiffness and load-carrying capacity and better dynamic properties since the inertia of the moving parts is considerably reduced. Among other architectures, spherical parallel manipulators have received some attention [9,10,11,12]. Alici and Shirinzadeh [7] proposed a spherical parallel manipulator, SPM, which is made of three identical moving legs and a fixed one, 3-SPS. Each of the three moving legs is made of SPS (spherical-prismatic-spherical) joints. The fixed leg joins the moving platform to the base with a passive spherical joint at the moving platform. The prismatic pairs are the actuated joints. Innocenti and Parenti-Castelli [13] ,Wohlhart [14] and Vertechy and Parenti-Castelli [10] have studied a spherical manipulator, 3-UPS, similar to Alici and Shirinzadeh [7]. The 3-UPS is also made of three identical moving legs and a fixed leg. Each of the three moving legs are made of UPS (universal-prismatic-spherical) joints. The fixed leg joins the moving platform to the base with a passive spherical joint at the moving platform. The prismatic pairs are the actuated joints. Both manipulators suffer workspace reductions due to the presence of the fixed leg.

One typical SPM, called agile eye [9,11], is used for orienting cameras and antennas. The pioneering work of Gosselin and Angeles [9], an over-constrained mechanism with actuated revolute joints, has contributed significantly to the subsequent development of SPMs. The agile eye is a successful technical application of a SPM nowadays, although it has a low lifting capacity.

2 Description of the Manipulator

The spherical star triangle (SST) parallel manipulator consists of a fixed spherical triangular base, ***P***, and a moving platform which is shaped like a spherical star, ***S***. The fixed base and the moving platform are connected via three legs. Each of the three moving legs is made of PRP (curved prismatic-revolute-curved prismatic) joints. We use the term curved prismatic to denote a motion that slides on a curved path. An example of this joint used in industry is Curviline which is a curved linear bearing [15]. The three branches of the spherical star and the three moving legs are each assumed to be identical resulting in a symmetrical geometry for the SST manipulator. The general model of this manipulator is depicted in Figure 1. The first curved prismatic joint which is also the motorized joint moves along circular arc, $P_i\,P_{i+1}$, located on the surface of the sphere. In practice, it is difficult to manufacture an actuated curved prismatic joint which moves on a circular arc. However, by closer inspection, one can see that each of the motorized joints can also be viewed as a revolute joint with its axis passing through the origin of the sphere. See Figures 2 and 3. In other words, each of the three legs can also be thought of being RRP (revolute-revolute-curved prismatic) joints. Therefore, to physically construct this manipulator we will build its legs with RRP joints. The physical model of this manipulator is depicted in Figure 3. To develop the mathematical model of the manipulator, first a sphere with center at $\boldsymbol{O}$ and a fixed spherical triangle, $P_1P_2P_3$, on its surface is considered. The unit vector $\mathbf{v}_i$ is defined along OP_i. Actuators stroke which can travel along the arc $P_i\,P_{i+1}$ are defined by angle γ_i. See Figures 1 and 2.

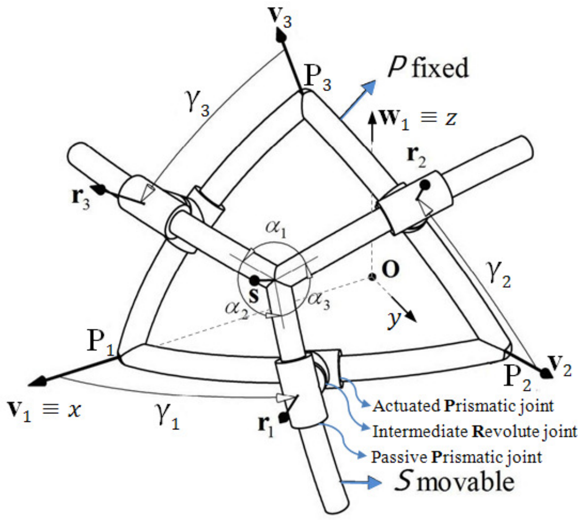

Figure 1 General Model of SST

The moving spherical star (MSS), $\boldsymbol{S}$, is next considered. The star is made of three arcs which are located on a surface of a second sphere. The first and the second spheres have the same center but the radius of the second sphere is slightly larger due to intermediate revolute joint. This difference should be minimized in order to increase the structural stiffness of the manipulator. The three arcs of MSS intersect at point E. The angle between these arcs, α_1, α_2 and α_3 can be manually selected by the robot designer to obtain the desired performance. Position of point E defines end-effector position. Direction OE can be defined by unit vector $\mathbf{s}$. See Figures 1 and 2. The arcs of the moveable star platform ER_i intersect the line which is along actuator links at the point R_i. Angular position of the actuators are defined by the unit vector $\mathbf{r}_i$. Direction of this unit vector is defined along OR_i. Furthermore, R_i is a joint which allows rotation about $\mathbf{r}_i$ axis as well as a rotation about the axis that passes through center of sphere, O, and is perpendicular to OER_i plane. See Figure 2.

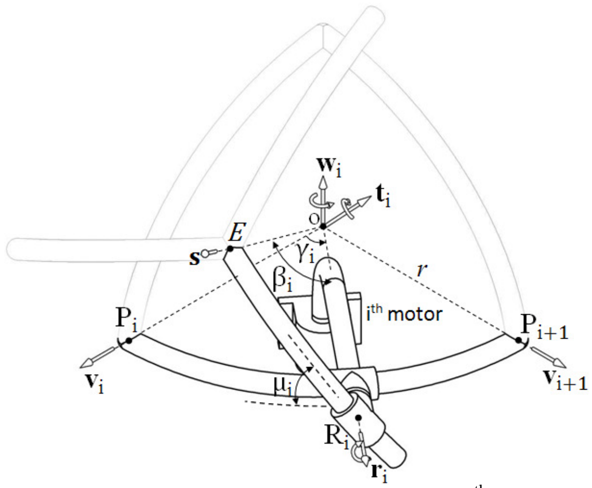

Figure 2 Parameters description of i^th leg

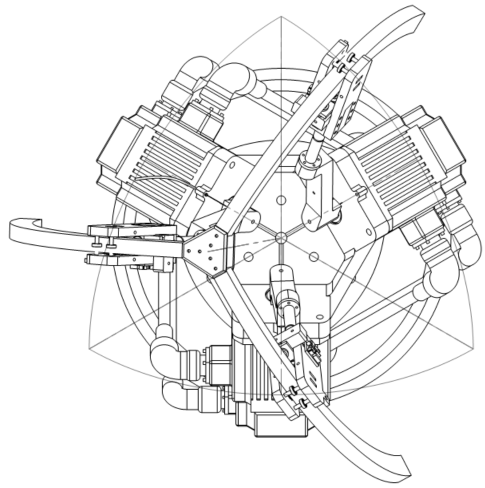
Figure 3 Physical Model of Zippy Wrist

3 Kinematics Analysis

The kinematic analysis of a spherical three-degree-of-freedom parallel manipulator and the solution of the inverse kinematic problem associated with this manipulator have been addressed in [1,2]. Polynomial solutions to the direct kinematic problem of the SST manipulator have been derived. It has been shown that this problem leads to a polynomial of degree 8. Expressions can be found for the coefficients of the polynomial. The maximum number of real solutions to the problem is 8. Given the physical structure of the manipulator, not all solutions can physically occur. In physical structure, only one solution can occur. We presented a procedure for selecting the admissible solution of the direct kinematics analysis in [16]. Also, solution of the inverse kinematics problem of the SST manipulator has been presented in a closed form [1].

For parallel mechanisms in general, the Jacobian matrix is used to establish a relation between generalized and actuators velocities as well as between generalized and actuators forces and couples. This relation for SST manipulator can be written as

$$\mathbf{J}\dot{\boldsymbol{\gamma}}+\mathbf{K}\boldsymbol{\omega}=\mathbf{0} \tag{1}$$

Where $\mathbf{J}$ and $\mathbf{K}$ are the direct and inverse kinematic problem Jacobian matrices for the SST manipulator, respectively. Moreover, $\dot{\boldsymbol{\gamma}}$ is the vector of actuated joint rates and $\boldsymbol{\omega}$ is the angular velocity of the moving platform, MSS. The Jacobian matrices $\mathbf{J}$ and $\mathbf{K}$ are obtained by velocity analysis and reported in [2] as follow:

$$\mathbf{J}=\begin{bmatrix} c_1 & 0 & 0 \\ 0 & c_2 & 0 \\ 0 & 0 & c_3 \end{bmatrix} \text{ and } \mathbf{K}=\begin{bmatrix} -(\mathbf{r}_1\times\mathbf{t}_1)^{\mathrm{T}} \\ -(\mathbf{r}_2\times\mathbf{t}_2)^{\mathrm{T}} \\ -(\mathbf{r}_3\times\mathbf{t}_3)^{\mathrm{T}} \end{bmatrix} \tag{2}$$

where $c_i=(\mathbf{r}_i\times\mathbf{t}_i)^{\mathrm{T}}\mathbf{w}_i$ for $i=1,2,3$

Equation 1 may be used to obtain a single Jacobian matrix for the manipulator $\mathbf{L}\dot{\boldsymbol{\gamma}}=\boldsymbol{\omega}$ where $\mathbf{L}=-\mathbf{K}^{-1}\mathbf{J}$.

4 Isotropic Design and Accuracy

Families of isotropic spherical parallel manipulators have been obtained through a detailed kinematic analysis [12,17] and the design of the manipulator presented here [2] is based on an optimization of these families of mechanisms. Mechanism control accuracy depends upon the condition number of the Jacobian matrices $\mathbf{J}$ and $\mathbf{K}$. Isotropic design of the SST manipulator can be obtained from

$$\mathbf{J}\mathbf{J}^{\mathrm{T}}=\sigma^2\mathbf{I}_{3\times3} \quad \text{and} \quad \mathbf{K}\mathbf{K}^{\mathrm{T}}=\tau^2\mathbf{I}_{3\times3} \tag{3}$$

Considering the above conditions and the geometry of the manipulator problem we find that isotropic designs are only possible if,

- The fixed spherical triangle is equilateral.
- The angle between sides of the moveable spherical star is 120 degrees.
- The end effector, point E, coincides with geometrical center of the fixed base equilateral triangle.

As shown by Strang [18], condition number is a measure of stability or sensitivity of a matrix to numerical operations. It is used in numerical analysis to estimate the error generated in the solution of a linear system of equations. In numerical analysis, a problem with a low condition number is said to be well-conditioned, while a problem with a high condition number is said to be ill-conditioned. When applied to manipulator Jacobian matrix, condition number will give a measure of accuracy of the Cartesian velocity of the end-effector. It also provides a measure of accuracy of static load acting on the end-effector. The condition number can also be used to evaluate the dexterity of a manipulator [19]. Therefore, we can use condition number as measure of accuracy. The condition number of Jacobian matrix can be written as

$$\kappa_{\mathbf{L}}=\frac{\sigma_{\mathrm{J,max}}}{\sigma_{\mathrm{J,min}}} \tag{4}$$

Where, $\sigma_{\mathbf{L},\max}$ and $\sigma_{\mathbf{L},\min}$ represent the maximum and minimum singular values of Jacobian matrix, respectively. $\kappa_{\mathbf{L}}$ can reach values from 1 to ∞. In order to bound κ_{J}, one may consider its inverse value defined by $\eta_{\mathbf{L}}=1/\kappa_{\mathbf{L}}$. The variable $\eta_{\mathbf{L}}$ is defined as kinematics conditioning index, KCI, and ranges between 0 and 1 (i.e., singular and isotropic configurations, respectively). This performance index is plotted for $\psi=0$ (Figures 4 and 5). As seen in Figure 5, there exists a minimum and a maximum value for KCI. These maximum and minimum values of KCI versus angle ψ are shown in Figures 6 and 7, respectively. Figure 6 shows maximum value of KCI, which is equal to 1, occurs at $\psi=0^{\circ}$. This configuration represents the isotropic configuration of the SST manipulator. Figure 7 shows that minimum value of KCI occurs at $\psi=60^{\circ}$ and $\psi=-60^{\circ}$. This value is equal to 0.412. As stated earlier, KCI value equal to zero represents singular configuration. Since the minimum value of KCI is higher than zero, the isotropic design of the SST manipulator is free of singularity.

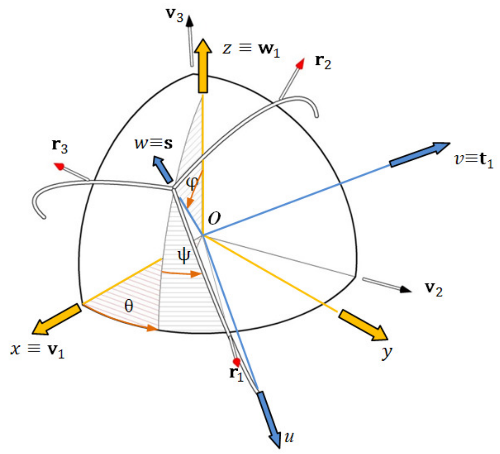

Figure 4 Degrees of freedom θ, φ, ψ

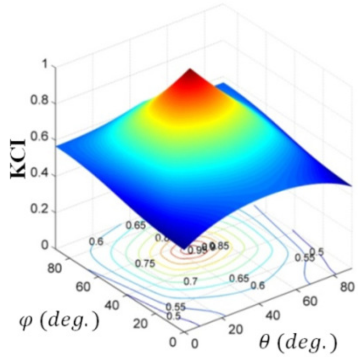

Figure 5 KCI of the SST manipulator on sphere for ψ=0°

Since the kinematics index is dependent on the Jacobian matrix, it is a local property of the mechanism. Kinematics conditioning index thus depends on the position and orientation of the end-effector as well as robot structure. Another performance index that covers the entire workspace is called global kinematics index (GCI). This type of index was introduced by Gosselin and Angeles [9]. This index is used to measure the global behavior of manipulator condition number. It computes the average of the kinematics conditioning index throughout robot workspace. Therefore, GCI can be written as

$$\mathrm{GCI}=\frac{\int_{\mathrm{w}}\eta_{\mathbf{L}}\,\mathrm{dw}}{\int_{\mathrm{w}}\mathrm{dw}} \tag{5}$$

Where w is the manipulator's reachable workspace. For the SST manipulator, this value is equal to 0.67.

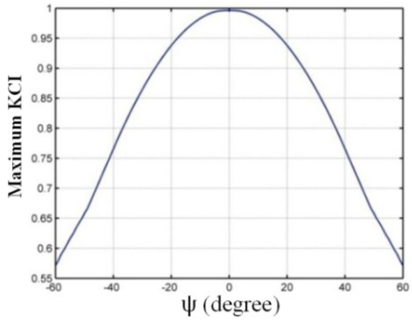

Figure 6 Maximum KCI versus angle ψ

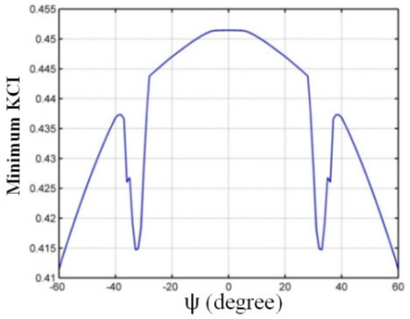

Figure 7 Minimum KCI versus angle ψ

5 Maximum angular velocity of the star

In this section, we define maximum angular velocity about x, y and z axes of the star. For this purpose, using maximum angular velocity of motors and Jacobian matrix, **L**, we can define

$$\begin{aligned} \omega_{x_{max}} &= \sum_{k=1}^{3} |\mathbf{L}_{1k} \dot{\gamma}_k| \\ \omega_{y_{max}} &= \sum_{k=1}^{3} |\mathbf{L}_{2k} \dot{\gamma}_k| \\ \omega_{z_{max}} &= \sum_{k=1}^{3} |\mathbf{L}_{3k} \dot{\gamma}_k| \end{aligned} \qquad (6)$$

Therefore, maximum angular velocity of MSS is

$$\omega_{max} = sqr({\omega_{x_{max}}}^2 + {\omega_{y_{max}}}^2 + {\omega_{z_{max}}}^2) \qquad (7)$$

The maximum workspace of SST manipulators is 1/8 of a sphere. Since maximum torque of motors are 5N.m and assuming motor can rotate a maximum of ±90 degrees, then maximum angular speed reached by motor is about 100rpm for an assumed trajectory. Considering a factor of safety of 5, we assume a maximum angular velocity for each motor is 500 rpm. These values are plotted for ψ = 0 in Figure 8.

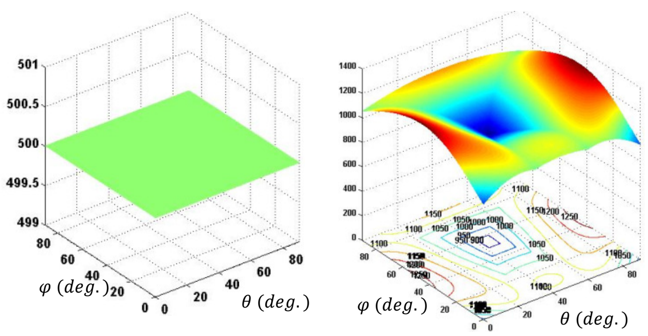

a) $\omega_{z_{max}}$ b) ω_{max}

Figure 8 Maximum angular velocity of the MSS for ψ=0°

6 Performance Specification

Desired performance is given in Table 1.

Table 1 Performance specification

End-Effector Angular Speed	~750 deg/sec
Load Carrying	1kg
Dimensions	R=350 mm for sphere
Star Accuracy - Angular	0.2~0.5 degrees
Workspace	1/8 of the sphere surface
Power	220V-Single phase

7 Joints Design

There are 3 similar sets of joints in the SST manipulator. The first revolute joint is the actuated joint which is simply satisfied with rotary motion of the motors shaft (γ_i). The second revolute joint provides the variable angle between star's arc and actuators arm (μ_i). The third special joint is a curvilinear prismatic joint which allows sliding motion of the star. Because we chose direct drive actuators, the design of the first revolute joint is simplified by a direct mount link. To avoid damage to the motor encoder due to possible axial impact during assembly as well as during high speed trajectories, a thrust bearing is placed between motor shaft and robot arm. This thrust bearing is mounted on the main motor holder structure. The axis of second revolute joint is perpendicular to the motor shaft. Actuator arm connects the motor joint to the second revolute joint. The actuator arm is equipped with two double bearings which allow the passive revolute action. The two double bearings are separated by about 4cm to insure alignment during high torque trajectories. The curvilinear joint is designed by use of miniature roller bearing on both sides of the star. Our design is advantages over the Curviline joint design by allowing higher lateral forces. Curviline, our initial and final design models are illustrated in Figure 9.

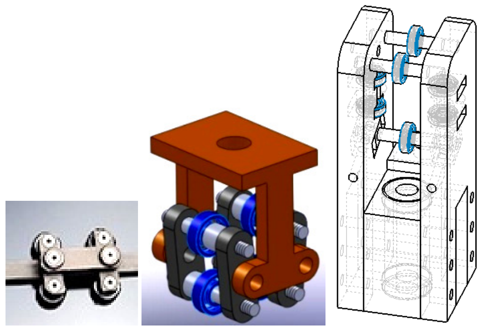
Figure 9 Curviline, Initial, Final Design (left to right)

8 Mechanical Components

8.1 Star

The configuration of the star is similar to a tripod with equal legs that are symmetrically connected together at one common end, Figure 10. Each leg has a constant radius arc with rectangular cross-section. The radial thickness of the cross-section is selected to be larger than its width, in order to allow higher bending resistance and have less deflection due to radial loading.

Maintaining specified radius is crucial for proper operation of the mechanism. Therefore, to avoid changes in the radius, the arcs are flame cut from an aluminium plate with a slightly larger dimension and then annealed to relieve its internal stresses. Afterwards, they undergo a CNC machining process to reach their exact dimensions and curvature.

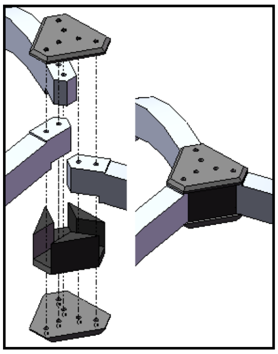

Figure 10 Star Joint

8.2 Motors Mount

This part holds motors and insures motor axes are perpendicular to each other. Therefore, like the star, it requires tight tolerances in order to assure proper operation of the mechanism. To do this, precision CNC machining on a solid block of aluminium is performed. To insure the perpendicularity and create three flat mounting surfaces for the motors, the block should undergo machining process all in one operation. Therefore, a 4 axis CNC machine is used and the aluminium block is remained in place during all of its machining process. To simplify the machining and reduce cost, we separated this part into two pieces which will bolt together. The second piece acts as a spacer from ground level.

8.3 Actuator Arms

Actuator links are oblique shaped so they do not interfere with each other at the center of the base sphere during the motion. One end of the link is connected to motor shaft and has a keyway, while the other end connects the Slider joint via a circular shaft extension. To manufacture this part, first the rough lateral shape is cut from a thick plate, and then the motor shaft hole is drilled and its keyway is cut using spark machining process. The other end is bolted to a circular extension. Assembled model of the whole structure is shown in Figure 18. The individual parts are listed in Table 2.

9 Electrical Setup

The motion control consists of the followings: A personal computer: A Pentium 4 main board with 2 Gigabytes of RAM for computationally intensive tasks. The encoder outputs are supplied to 1784U PCI cards manufactured by Advantech Co. The desired torque is calculated by the robot dynamic algorithms and supplied to the driver TSTA-30C by the PCI1710 D/A card from the Advantech Co. The motors are AC servos, model number TSB1310 supplied by TECO Electro Devices Co. These motors provide the maximum of 5N.m of torque and have a maximum speed of 2000 RPM. Power consumption of each motor is 1KW with the maximum current of 5Amps, and uses Single/three phase 220v AC input power and its mechanical time constant is 1.14ms. The motor drivers are TSTA-30C which are also manufactured by TECO Electric Devices Co. These drivers have the capability to offer torque mode, position mode and also speed mode. The three drivers are connected through inter-connect terminal boards to two additional inter-connect terminal boards which are themselves connected to the aforementioned PCI cards.

Table 2 – List of Mechanical Components of Zippy Wrist

Part Name	Material	Process	Weigh
Base	St	Machining	86 kg
Motors Stand	St	CM	34.1 kg
Motors Holder	Al	CM	4.6 kg
Motors	Model: TSB1310 by TECO		
Actuator Arm Links	Al	CM	0.35 kg
Extension Shaft I	Al	CM	0.03kg
Extension Shaft II	Al	CM	0.03 kg
Mechanical Fuse	Al	Machining	-
Slider Frames	St	CM / WC	0.47 kg
Slider Holder	Al	CM	0.22 kg
Star's Arc	Al	CM / AN / FC	0.87 kg
Star Holder	Al	CM	0.2 kg
Star Holder Cap	Al	CM	0.1 kg

St: Steel, Al: Aluminium Alloy 2024, CM: CNC Machining
WC : Wire cut, AN: Annealing, FC: Flame cut

10 Workspace

Robot workspace is an important criterion in evaluating manipulator performance. Determination of the workspace can be performed either by a numerical discretization of the Cartesian space or by the derivation of analytical expressions of the boundaries of the workspace [20,21]. The theoretical, reachable, and actual workspace of the SST manipulator is obtained. For theoretical workspace, we assume zero volume for joints and zero thickness for links. This workspace is reported in [1] and is determined by numerical discretization of the Cartesian space on sphere. Workspace of the SST manipulator depends on the value of ψ angle and is plotted for two values of ψ in Figures 11.

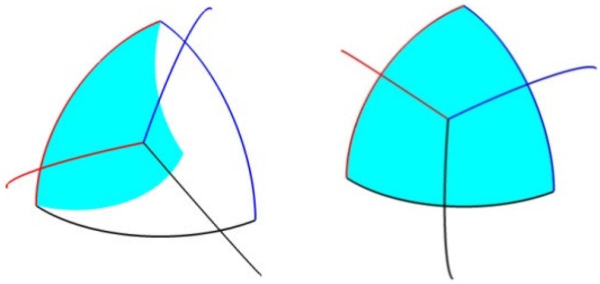

$\psi = 45^\circ$ $\psi = 0^\circ$

Figure 11 Theoretical workspace with respect to ψ

The reachable workspace of this manipulator is one-eighth area of the sphere. However, in practice volume of joints and links limit the ideal workspace. The actual workspace of this robot depends on joints, links and star dimensions and their collision.

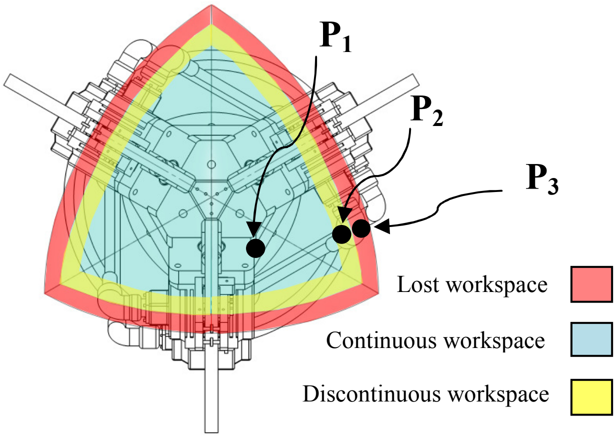

Figure 12 Actual workspace division with respect to ψ

As it is shown in Figure 12 we lose the red band from the (θ, φ) workspace due to curvilinear joint dimension and also thickness of the arcs. Moreover, at vicinity of the red band we have a discontinuous domain available for ψ angle due to collision. Figure 13 shows this issue. The red area is where the end-effector cannot reach regardless of the value for ψ. The yellow area is where the end-effector can reach with some values of ψ. However, the ψ values are not necessarily continuous. For example, points P as shown in Figure 12 allow the followings:

Point P1: θ = 60°, φ = 70°, ψ = [-70 +60]°
Point P2: θ = 83°, φ = 70°, ψ = [-71 -65] and [20 33]°
Point P3: θ = 87°, φ = 70°, ψ = None

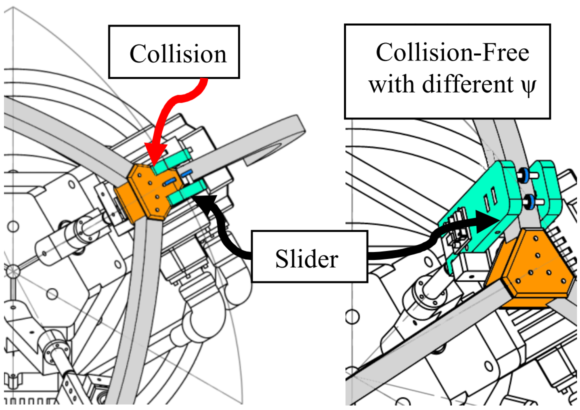

Figure 13 Discontinuity in ψ domain example

11 Sensors and Microswitches

The limit switches are used as emergency stop as well as aid in the homing process. Therefore, in addition to micro switches used for homing process, additional micro switches are used to avoid component collision in case of failure of the control system. During motion, collisions may occur if the followings collide:

1- Star and sliders collision as well as their separation
2- Adjacent sliders at workspace corners
3- Any two actuator arm if they both travel 45 degrees in opposite directions from home position
4- Star with steel base
5- Arms with adjacent motor at their extreme travel

To detect all five types of collisions at least 6 microswitches are needed. Rolling contact microswitches is selected for this purpose. See Figure 17. Since the slider is a moving joint and would cause problems with wiring, a wireless module is implemented. Additionally 3 fibre optic sensors are necessary for homing strategy due to necessity of high position accuracy and repeatability.

12 Finite Element Analysis

A commercial finite element software is used to develop a finite element model of the Star. Two element types are used in this modelling: Solid45 and 3D mass. For this analysis, we add 3kg payload to the star at end-effector point (point E) and rotate the star about the unit vector s by 500 rpm. The star is made of aluminium with module of elasticity and Poisson's ratio of 70 GPa and 0.33, respectively. Deformation and Von Mises stress of the star are shown in Figures 14 and 15.

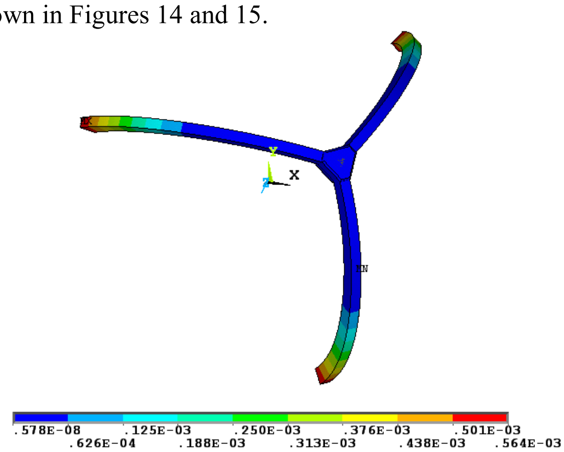

Figure 14 Displacement of the star (meter)

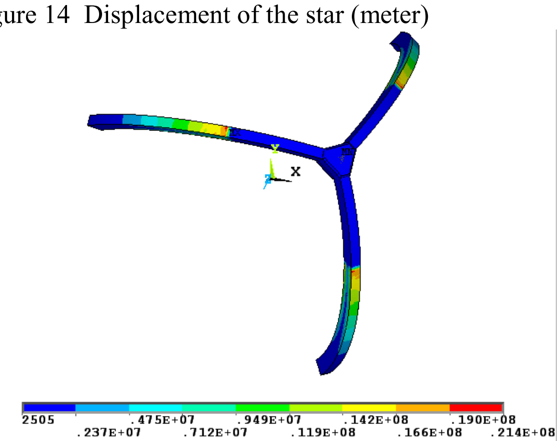

Figure 15 Von Mises stress of the star (Pa)

Furthermore, the curvilinear slider joint is modelled using another commercial solid modelling software. The model underwent a finite element analysis and the displacement contour is illustrated in Figure 16. The simulation assumes a 5 N.m torque is applied by a motor shaft which transmits through the actuator arms to the slider mechanism. Material used for all parts in the slider mechanism is assumed to be aluminium alloy 1060.

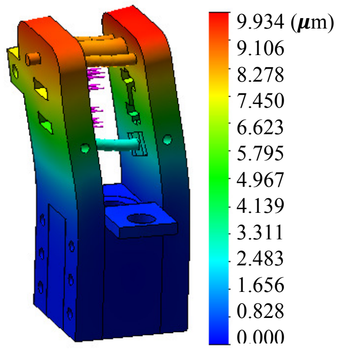

Figure 16 Displacement contour of the slider joint FEM

13 Dynamics Simulation

The theoretical dynamic equations, using simplified component geometries, have previously been implemented using Matlab software [4]. In this paper, the complete detail model undergoes a dynamic simulation. Each kinematic chain of the 3-RRP includes two revolute and one curved prismatic joints. The two revolute joints are defined with a simple revolute joint. The curved prismatic joint is not predefined in commercial solid modelling software. Instead, this joint is defined by its restricted degrees of freedom. See Figure 17. Therefore, the curvilinear joint is defined using lateral and radial restrictions. Only one radial restriction is defined for all three legs which tolerate all radial forces between star and the three sliders.

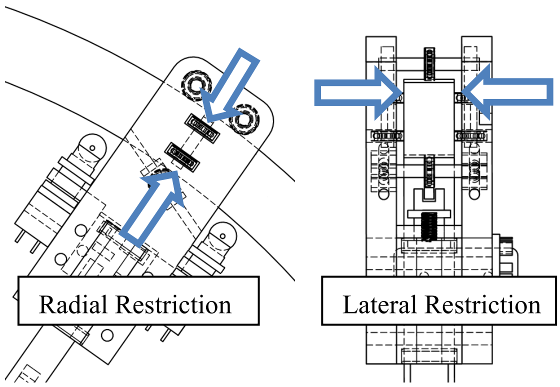

Figure 17 Kinematical curvilinear joint definition

A simple circular trajectory is considered. Then, the end-effector orbits around its home position by drawing a circle using the following equations

$$\theta = \tan^{-1}(s'_{y'}/s'_{x'}), \quad \varphi = \cos^{-1} s'_{z'}, \quad \psi = 0 \qquad (8)$$

The inverse kinematic solution is obtained by reading motors rotary positions. To achieve the same circular motion using Cartesian coordinate xyz, shown in Figure 18, the following equation is used

$$s_x = 0.1\sin(2\pi t)\ m \ , \ s_y = 0.1\cos(2\pi t)\ m \qquad (9)$$

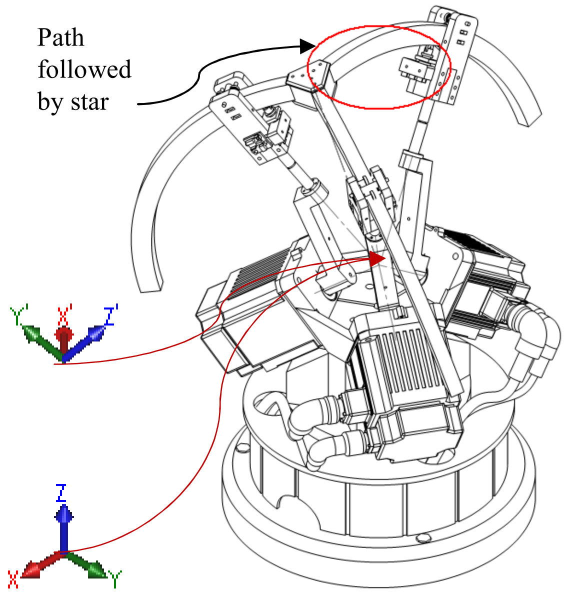

Figure 18 Dynamic Simulating Model

Motor torques during the specified trajectory are recorded and shown in Figure 19 for a payload of 1 kg on the end-effector and gravity along Z-direction. During this trajectory motor speed reaches a maximum of 15rpm.

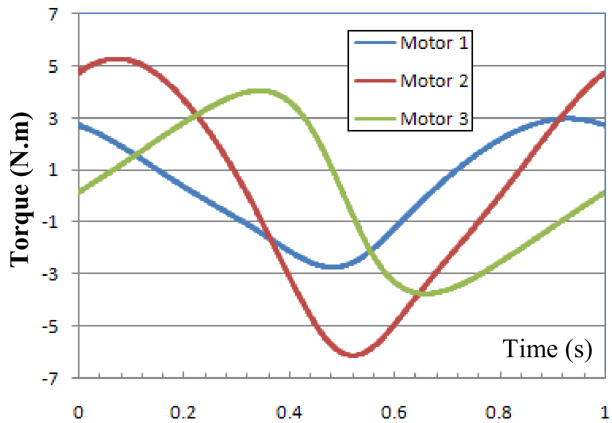

Figure 19 Motor torques as the result of the simulation

14 Conclusion

This paper has presented an overview of kinematics, mechanical design process and control architecture for the 3-RRP parallel manipulator at Ferdowsi University of Mashhad. The 3-RRP robot is a spherical parallel manipulator, also called Zippy Wrist, capable of orienting a tool or a workpiece. The paper presented an overview of the isotropic design and accuracy of this manipulator. For the mechanical design, we selected the isotropic design because it is the superior design. The joints design as well as a new curved prismatic joint were introduced. Motor mount and actuator arm to insure proper alignment were discussed. The lost, continuous and discontinuous workspace of the manipulator was calculated. It was shown that due to conflict of mechanical components, the actual workspace is smaller than the reachable. Next a finite element model of the Star was developed. The model showed insignificant deflection of the star. Furthermore, the curvilinear slider joint was modelled using another commercial software. Results also indicated insignificant deflection at the joint. Finally, a dynamics simulation was performed and motor torques were measured. Results indicated that motor can produce the required torques. The Zippy wrist design has benefited from many modelling. However, since the unit is not built yet, the final performance cannot be determined. One thing we have learned thus far is that, despite our desire to use direct drive motors to improve robot accuracy, we must use gear box. Despite its negative effect, the gear reduction allows us to further improve dynamic performance, load carrying and enables us to better use control system capabilities. For future works, the robot will be physically constructed.

15 Literature

[1] Enferadi J., Akbarzadeh Tootoonchi A., Accuracy and Stiffness Analysis of a 3-RRP Spherical Parallel Manipulator, Robotica, Accepted paper (2009)

[2] Enferadi J., Akbarzadeh Tootoonchi A., A Novel Spherical Parallel Manipulator: Forward Position Problem, Singularity Analysis and Isotropy Design, Robotica, 2009, 27: pp. 663–676.

[3] J. Enferadi, A. Akbarzadeh Tootoonchi, " A Novel Approach for Forward Position Analysis of a Double-Triangle Spherical Parallel Manipulator ", European Journal of mechanics \ A solid, Accepted paper, 2009.

[4] Enferadi J., Akbarzadeh Tootoonchi A., Inverse Dynamics Analysis of a General Spherical Star-Triangle Parallel Manipulator Using Principle of Virtual Work, Nonlinear Dynamics, Revised paper, 2009.

[5] D. Chablat, and J. Angeles, The Computation of All 4R Serial Spherical Wrists With an Isotropic Architecture, ASME J. Mech. Des., 125(2), pp.275–280 (2003).

[6] J.M. Wiitala and M.M. Stanisic, Design of an Overconstrained and Dexterous Spherical Wrist, ASME J. Mech. Des., 122(3), pp. 347–353 (2000).

[7] G. Alici and B. Shirinzadeh, Topology optimisation and singularity analysis of a 3-SPS parallel manipulator with a passive constraining spherical joint, Mechanism and Machine Theory, vol. 39, pp. 215–235 (2004).

[8] M. Karouia and J.M. Herve´, A Three-dof Tripod for Generating Spherical Rotation, Advances in Robot Kinematics, Lenarcic, J. and Stanisic, M. M., eds., Kluwer Academic Publishers, Netherlands, pp. 395–402 (2000).

[9] Gosselin C.M., Angeles J., The optimum kinematic design of a spherical three-degree-of-freedom parallel manipulator, ASME Journal of Mechanisms Transmission and Automation in Design, 111 (2) (1989): pp. 202–207.

[10] R. Vertechy and V. Parenti-Castelli, Real-Time Direct Position Analysis of Parallel Spherical Wrists by Using Extra Sensors, ASME J. Mech. Des., vol. 128, pp. 288-294 (2006).

[11] Gosselin C.M., Pierre E., and Gagne M., On the development of the agile eye, IEEE Robotics &Automation Magazine, December, (1996), pp. 29-37

[12] C. Gosselin and E. Lavoie, On the kinematic design of spherical three-degree-of-freedom parallel manipulators, The International Journal ofRobotics Research, Vol. 12, No. 4, pp. 394-402, 1993.

[13] C. Innocenti and V. Parenti-Castelli, Echelon Form Solution of Direct Kinematics for the General Fully-Parallel Spherical Wrist, Mechanism and Machine Theory, 28(4), pp. 553–561 (1993).

[14] K. Wohlhart, Displacement Analysis of the General Spherical Stewart Platform, Mechanism and Machine Theory, 29(4), pp. 581–589 (1994).

[15] http://www.rollonbearings.com/linearalrails.html

[16] Enferadi J., Akbarzadeh Tootoonchi A Virtual Work Based Algorithm for Solving Direct Dynamics Problem of a 3-RRP Spherical Manipulator Submitted to Journal of Intelligent Robotic System March. 2010

[17] C. Gosselin and J.-F. Hamel, The agile eye: a high-performance three-degree-of-freedom camera-orienting device, Proceedings of the IEEE International Conference on Robotics and Automation, pp. 781-786, San Diego, 1994.

[18] G. Strang, "Linear Algebra and its Application", Academic Press, New York, 1976.

[19] J.K. Salisbury, J. Graig, "Articulated hands: force control and kinematic issues", The International Journal of Robotics Research, 1 (1) (1982), 4-17.

[20] V. Kumar, Characterization of Workspaces of Parallel Manipulators, Journal of Mechanical Design, 114(3) (1992), 368–375.

[21] J.P. Merlet, C.M. Gosselin, N. Mouly, Workspaces of Planar Parallel Manipulators, Mechanism and Machine Theory, 33 (1998), 7–20.